INTERNATIONAL JOURNAL FOR NUMERICAL METHODS IN FLUIDS
Int. J. Numer. Meth. Fluids 2009; **59**:1217–1240
Published online 3 December 2008 in Wiley InterScience (www.interscience.wiley.com). DOI: 10.1002/fld.1871

An arbitrary Lagrangian–Eulerian method based on the adaptive Riemann solvers for general equations of state

Baolin Tian*,†, Weidong Shen, Song Jiang‡, Shuanghu Wang and Yan Liu

Institute of Applied Physics and Computational Mathematics, Beijing 100088, China

SUMMARY

Approximate or exact Riemann solvers play a key role in Godunov-type methods. In this paper, three approximate Riemann solvers, the MFCAV, DKWZ and weak wave approximation method schemes, are investigated through numerical experiments, and their numerical features, such as the resolution for shock and contact waves, are analyzed and compared. Based on the analysis, two new adaptive Riemann solvers for general equations of state are proposed, which can resolve both shock and contact waves well. As a result, an ALE method based on the adaptive Riemann solvers is formulated. A number of numerical experiments show good performance of the adaptive solvers in resolving both shock waves and contact discontinuities. Copyright © 2008 John Wiley & Sons, Ltd.

Received 7 January 2008; Revised 27 May 2008; Accepted 27 May 2008

KEY WORDS: adaptive Riemann solvers; Godunov-type scheme; ALE methods; general equations of state; shock wave; contact discontinuity

1. INTRODUCTION

Compressible multi-material flows can be found in a variety of science and engineering problems, and they are characterized by the interaction of shock waves and material interfaces. Development of numerically accurate and computationally efficient algorithms for multi-material flow simulations remains one of the unresolved issues in computational fluid dynamics.

Artificial viscosity methods and Godunov-type methods are two main methods for compressible flows with shock waves. The introduction of the concept of artificial viscosity by von Neumann

*Correspondence to: Baolin Tian, Institute of Applied Physics and Computational Mathematics, No. 6 Huayuan Road, Haidian District, Beijing 100088, China.
†E-mail: tian_baolin@iapcm.ac.cn
‡E-mail: jiang@ipacm.ac.cn

Contract/grant sponsor: National Basic Research Program; contract/grant number: 2005CB321700
Contract/grant sponsor: NSFC; contract/grant number: 10225105
Contract/grant sponsor: Science Foundation of CAEP; contract/grant number: 20060648
Contract/grant sponsor: Key Lab Foundation; contract/grant number: 9140C690101070C69

and Richtmyer in 1950 permitted for the first time the development of practical numerical methods for problems involving strong shock waves [1]. The basic idea was to spread the thickness of a shock wave over several computational cells, allowing the numerical method to resolve, and therefore 'capture' the shock wave. The real utility and simplicity of the method account for its widespread and continuing popularity. The main drawback of the method is that in practical usage it could produce either overly thick or oscillatory shock profiles.

In 1959, a different, alternative method was developed by Godunov *et al.* [2]. He proposed to consider all quantities in a computational cell to be constant at the start of the time step, given by the cell-averaged value of the conservative variables, and to resolve the resultant discontinuities at cell edges by the solution of a Riemann problem, which thus plays a key role in the Godunov method. The advantage of this method is the clear picture of the interactions involved and the absence of any arbitrary parameters. The method naturally and automatically handles shock waves, interfaces between different materials, and predicts cavitation should it occur. In practice, the method is characterized by nearly optimally thin shocks, typically one to three cells wide [3]. From the mathematical point of view, it has the desirable properties of monotonicity and the physically correct flow of information. The main drawback of the method, which has limited its widespread use, is the difficulty and the high cost of solving the (nonlinear) Riemann problem exactly, especially for materials with complex equations of state, which are frequently available only in tabular form.

The use of the Godunov method has recently attracted new interest in the field of computational fluid dynamics. Since a Riemann solver is a key component of the Godunov method, it has always been a challenging and attracting problem to find an efficient and accurate approximate Riemann solver in the development of Godunov-type numerical methods.

One of the first approximate Riemann solvers, by Godunov *et al.* [2], was to replace all waves in the Riemann problem by sound waves, in cases when the waves were expected to be weak. Therefore, this scheme is also called the weak wave approximation method (WWAM). With the simplification of only ideal gases encountered, several successful linear approximations have been developed; among them are the methods according to Enquist and Osher [4], Roe [5], Toro [6] and so on.

As for the Riemann solvers for general equations of state, the early WWAM scheme exhibits its deficiency when encountering strong shock waves or contact discontinuities, which could be smeared severely. Shui *et al.* developed an approximate Riemann solver, called MFCAV, see [7]. The MFCAV scheme attempts a compromise by combining the merits of both the WWAM scheme and artificial viscosity methods and can resolve contact discontinuity quite sharply. Dukowicz proposed a non-iterative Riemann solver in 1985 [3], which is characterized by only two material-dependent parameters. Dukowicz's scheme (DKWZ) is a two-shock approximation Riemann solver, where both left and right waves are approximated by the shock relation. Thus, DKWZ scheme shows good performance on strong shock waves. Miller and Puckett [8] made an important improvement to Dukowicz's Riemann solver. Although a similar quadratic $P(U)$ function is employed in both [3, 8], the local coefficients for weak and strong waves are used in Miller and Puckett's Riemann solvers through local evaluation of the derivatives of the equations of state, whereas Dukowicz takes the strong wave coefficient to be a global constant. This difference gives the method in [8] second-order accuracy in regions of smooth flow. These methods were further extended by Rider [9], who improved the approach by adding an adaptive form of the evaluation of the derivatives of the equations of state.

van Leer took another direction to develop the Godunov method [10]. He proposed to represent the distribution of variables in a cell by piecewise linear segments, limited in such a way as to

DOI: 10.1002/fld

preserve monotonicity. The remaining discontinuities at cell edges are again to be resolved by the solution of a Riemann problem. This modification improves the formal accuracy of Godunov's method to second order in the smooth regions of flow. Further developments along this line, e.g. the PPM scheme, also in the context of ideal gas equations of state, are represented by the study of Colella and Woodward [11].

As is well known, the Riemann solvers based on general equations of state have more practical applications than those only suitable for ideal gases, and they can be used in the simulation of many practical multi-material compressible flows. The above-mentioned Riemann solvers for general equations of state have their own advantage and disadvantage. Some can resolve shocks well, and others perform better in capturing contact discontinuities. Thus, in this paper we first compare and analyze the numerical features of the MFCAV, DKWZ and WWAM schemes, based on their resolution for shock waves and contact discontinuities. Then, we propose new adaptive Riemann solvers for general equations of state by combining the merits of these three schemes. Moreover, for the sake of completeness, an ALE method is formulated for two-dimensional compressible Euler equations based on our adaptive Riemann solvers and the Godunov method. Numerical tests confirm that our adaptive solvers perform well in resolving both shock waves and contact discontinuities.

This paper is organized as follows. In Section 2, we set up the control equations and the discretization methods. In Section 3, we describe how to construct the adaptive Riemann solvers for general equations of state. In Section 4, some numerical tests are presented, which demonstrate the good resolution of the new Riemann solvers for both shocks and contact discontinuities. In Section 5, we draw our conclusion.

2. CONTROL EQUATIONS AND NUMERICAL METHOD

2.1. Physical model and control equations

Traditional Lagrangian methods for compressible multi-material flows can track material interfaces clearly, while they often fail to deal with large mesh distortions. On the contrary, Eulerian methods find it difficult to treat mixed cells even with their robustness. The arbitrary Lagrangian–Eulerian (ALE) methods attempt a compromise by combining the merits of both Lagrangian and Eulerian methods and play an increasingly important role in the computation of multi-material flows, such as large slip flow, fluid–structure interactions, free surfaces, internal interfaces and so on [7, 12–19].

As aforementioned, in this paper we first construct new adaptive Riemann solvers by combining the merits of WWAM, DKWZ and MFCAV solvers. Then, with the help of the adaptive solvers and for the sake of completeness, we describe a Godunov-type method in ALE formulation for compressible multi-material flows. We will restrict our study to the two-dimensional Euler equations. The three-dimensional case can be dealt with in the same manner.

The two-dimensional Euler equations in conservative form can be expressed as follows:

$$\begin{aligned}
&\frac{\mathrm{d}}{\mathrm{d}t}\int_{\Omega(t)}\rho\,\mathrm{d}V+\oint_{\partial\Omega(t)}\rho(\mathbf{u}-\mathbf{u}_{\mathrm{G}})\cdot\mathbf{n}\,\mathrm{d}s=0\\
&\frac{\mathrm{d}}{\mathrm{d}t}\int_{\Omega(t)}\rho\mathbf{u}\,\mathrm{d}V+\oint_{\partial\Omega(t)}\rho\mathbf{u}(\mathbf{u}-\mathbf{u}_{\mathrm{G}})\cdot\mathbf{n}\,\mathrm{d}s=-\int_{\Omega(t)}\mathrm{grad}\,p\,\mathrm{d}V\\
&\frac{\mathrm{d}}{\mathrm{d}t}\int_{\Omega(t)}\rho E\,\mathrm{d}V+\oint_{\partial\Omega(t)}\rho E(\mathbf{u}-\mathbf{u}_{\mathrm{G}})\cdot\mathbf{n}\,\mathrm{d}s=-\oint_{\partial\Omega(t)}p\mathbf{u}\cdot\mathbf{n}\,\mathrm{d}s
\end{aligned}\tag{1}$$

DOI: 10.1002/fld

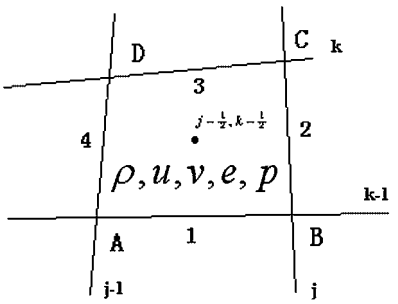

Figure 1. Variables on computational mesh.

where the subscript $\Omega(t)$ is the moving control volume, $\mathbf{u}=(u,v)^{\mathrm{T}}$ is the velocity, $\mathbf{u}_{\mathrm{G}}$ is the specified velocity of grid movement, $E=e+\frac{1}{2}\mathbf{u}\cdot\mathbf{u}$ is the total energy and ρ is the density. The pressure is given by the equation of state $p=p(\rho,e)$.

2.2. ALE method

In our ALE formulation, the computation is performed on a regular (non-overlapping) union of topologically rectangular submeshes, called blocks, each composed of arbitrary quadrilateral cells. As shown in Figure 1, all variables, including velocity, are defined at the center of mesh cells.

The ALE computation is performed in two phases: Lagrangian phase and rezone–remap phase. In the Lagrangian phase, the computational cell boundaries are assumed to move with the local flow velocity, and this can be implemented by solving the two-dimensional conservative equation (1) without convection terms. The rezone–remap phase is an interpolation procedure that transfers the physical variables from one computational mesh to another, i.e. from the Lagrangian phase mesh to the mesh of the next time step by rezoning. Generally, remapping is implemented in a conservative manner at any time in the computation that such a transfer is desired. In fact, the rezone–remap is independent of the Lagrangian phase. For simplicity, in this paper we shall restrict our main attention to the Lagrangian phase.

2.2.1. Discretization of the Lagrangian phase. Conservative computational methods are generally based on the control volume formulation of the conservative equations. In the Lagrangian phase, the following equations are solved numerically:

$$\begin{aligned}
&\frac{\mathrm{d}}{\mathrm{d}t}\int_{\Omega(t)}\rho\,\mathrm{d}V=0\\
&\frac{\mathrm{d}}{\mathrm{d}t}\int_{\Omega(t)}\rho\mathbf{u}\,\mathrm{d}V=-\int_{\Omega(t)}\mathrm{grad}\,p\,\mathrm{d}V\\
&\frac{\mathrm{d}}{\mathrm{d}t}\int_{\Omega(t)}\rho E\,\mathrm{d}V=-\oint_{\partial\Omega(t)}p\mathbf{u}\cdot\mathbf{n}\,\mathrm{d}s
\end{aligned}\tag{2}$$

Here we denote the cell mass by $M=\int_{\Omega(t)}\rho\,\mathrm{d}V$. In the Lagrangian phase M remains constant. Considering the quadrilateral cell ABCD shown in Figure 1 and using the Green formula for

DOI: 10.1002/fld

momentum equation, we discretize Equation (2) as follows:

$$\begin{aligned} M\frac{\mathbf{u}^{\mathrm{L}}-\mathbf{u}^{n}}{\Delta t} &= -\oint_{\partial\Omega(t)} p^{*}\mathbf{n}\,\mathrm{d}s = -\sum_{i=1}^{4} p_i^4 S_i \mathbf{n}_i \\ M\frac{E^{\mathrm{L}}-E^{n}}{\Delta t} &= -\oint_{\partial\Omega(t)} p^{*}\mathbf{u}^{*}\cdot\mathbf{n}\,\mathrm{d}s = -\sum_{i=1}^{4} p_i^4 S_i \mathbf{u}^{*}\cdot\mathbf{n}_i \end{aligned} \tag{3}$$

where S_i denotes the ith cell edge of the four edges of the quadrilateral cell ABCD, $\mathbf{n}_i$ is the unit outward normal of the ith edge, and $p^{*}, \mathbf{u}^{*}\cdot\mathbf{n}$ are the pressure and outward normal velocity, respectively. $p^{*}, \mathbf{u}^{*}\cdot\mathbf{n}$ can be computed from the value of the conservative variables at the cell center by an approximate Riemann solver, which will be discussed in detail in the following section. In a word, we can obtain the Lagrangian velocity $\mathbf{u}^{\mathrm{L}}$ and total energy E^{L} by Equation (3).

Moreover, it is necessary to determine the position of mesh vertices in the Lagrangian phase. Thus, the velocity of mesh vertex movement needs to be computed in order to appropriately move the mesh in a Lagrangian calculation. In this paper, a simple and robust least-square algorithm is used to compute the vertex velocity from the edge-normal velocity, $\mathbf{u}^{*}\cdot\mathbf{n}$ (see [13]). We take the normal projection of the vertex velocity to any one of the adjacent edges to be the velocity computed by solving the Riemann problem corresponding to that edge. This results in an overdetermined system of equations, and then the vertex velocity is determined by solving the following overdetermined system using the least-square algorithm:

$$\mathbf{u}_{*}^{\mathrm{L}}\cdot\mathbf{n}_i = u_i^{*}, \quad i = 1, 2, 3, 4, \ldots \tag{4}$$

In Equation (4) $\mathbf{u}_{*}^{\mathrm{L}}$ is the (Lagrangian) vertex velocity to be solved, and u_i is the edge-normal velocity. This least-square-based method of determining the vertex velocity is almost the same as in the CAVEAT code [13] except the calculation of the weights. Here a length weight has been adopted, where the length is the length of the edge connected to the vertex. Although, as Dukowicz [20], Shashkov and others pointed out, the least-square-based method could lead to spurious vorticity error when a mesh becomes distorted, continuous rezoning and remapping may be adapted to avoid severe mesh distortions in many cases. Hence, the least-square-based method of determining the vertex velocity works well in a number of problems including the numerical examples in this paper. An improved method of determining the vertex velocity similar to the method of subzonal pressures [21] has been studied in our ALE method, but more detailed analysis is necessary in the future study.

With the vertex velocity, the Lagrangian position of mesh points are computed as follows:

$$\mathbf{X}^{\mathrm{L}} = \mathbf{X}^{n} + \mathbf{u}_{*}^{\mathrm{L}}\Delta t$$

Thus, we can compute the cell volume, density, internal energy, and the cell pressure can be obtained by the equation of state. Then, a whole Lagrangian phase computation is completed.

2.2.2. Rezone and remap phase

2.2.2.1. Rezone. After the Lagrangian phase, the Lagrangian mesh may become distorted. Hence, it is necessary to rezone the mesh to improve mesh quality. In the CAVEAT code [13], the whole computation region is remeshed and the material interfaces are restored by removing the

DOI: 10.1002/fld

velocity component normal to the interfaces, whereas in our ALE method, material interfaces are determined in Lagrangian motion at first, and the rezoning is performed in each material region, such that nodes on interfaces can be redistributed to improve the mesh quality. An algorithm for adaptive mesh generation based on the following elliptic equations is adopted to implement the rezoning [22]:

$$\begin{aligned} \alpha x_{\xi\xi} - 2\beta x_{\xi\eta} + \gamma x_{\eta\eta} &= P \\ \alpha y_{\xi\xi} - 2\beta y_{\xi\eta} + \gamma y_{\eta\eta} &= Q \end{aligned} \tag{5}$$

$$\alpha = x_\eta^2 + y_\eta^2, \quad \beta = x_\xi x_\eta + y_\xi y_\eta, \quad \gamma = x_\xi^2 + y_\xi^2$$

where P and Q are two source terms to control the mesh density.

2.2.2.2. Remap. After rezoning, the conservative variables $(\rho, \rho\mathbf{u}, \rho E)$ computed in the Lagrangian phase have to be remapped from the Lagrangian mesh to the new rezoned mesh. The remapping here makes use of the conservative advection terms in the conservation laws and is called continuous remapping. The remapping is implemented by the following advection equation:

$$\frac{\mathrm{d}}{\mathrm{d}t}\int_\Omega q\,\mathrm{d}V = \oint_{\partial\Omega} q\,\mathbf{u}_\mathrm{R}\cdot\mathbf{n}\,\mathrm{d}s \tag{6}$$

where q is any one of the conservative variables per unit volume, and $\mathbf{u}_\mathrm{R}$ is the velocity of the fluid relative to the mesh. In our paper, Equation (6) is solved by a second-order MUSCL scheme [13, 23], where a minmod limiter is used to maintain the monotonicity.

Now, we have obtained all necessary physical variables at the new time step, and a complete ALE step is finished.

As for the treatment of boundary conditions, ghost cells outside the computational domain are disposed. In the ghost cells, the cell density, fluid velocity and pressure are specified according to different boundary conditions. For example, for the free-surface boundary condition, the density of ghost cells are set to be zero, and velocity and pressure in ghost cells are set to be continuous to adjacent cells in the computational domain.

3. ADAPTIVE RIEMANN SOLVERS

In Equation (3), the pressure and normal velocity, p^*, u^* remain unknown, and now Riemann solvers are applied to obtain their values. On each cell edge, a local Riemann problem can be constructed with two adjacent cell values as the initial data of the Riemann problem. Known the pressure and normal velocity on a cell edge, Equation (3) can be integrated conveniently.

Before giving our new adaptive Riemann solvers, we first present three approximate Riemann solvers, WWAM, MFCAV and DKWZ mentioned in Section 1. As shown in Figure 1, we take the edge j to construct a local Riemann problem as an illustration; the value of the conservative variables at the cell center of the cells $j-\frac{1}{2}$ and $j+\frac{1}{2}$ will be taken as the initial data of the Riemann problem to compute p^*, u^*.

DOI: 10.1002/fld

3.1. Review of three approximate Riemann solvers for general equations of state

3.1.1. Weak wave approximation method (WWAM) [2]

$$u^* = \frac{(\rho c u)_L + (\rho c u)_R - (p_R - p_L)}{(\rho c)_L + (\rho c)_R}$$

$$p^* = \frac{(\rho c)_L p_R + (\rho c)_R p_L - (\rho c)_L (\rho c)_R (u_R - u_L)}{(\rho c)_L + (\rho c)_R}$$

In the above formula, c is the cell sound speed, and u_L, u_R is the normal velocity component on the edge j of the two adjacent cells. In fact, the WWAM scheme is an average for the velocity and pressure based on the sound impedance, and all waves in the Riemann solver are replaced by sound waves with the assumption that the waves are expected to be weak.

3.1.2. MFCAV scheme [7]

$$u^* = \frac{(\rho c u)_L + (\rho c u)_R}{(\rho c)_L + (\rho c)_R} - \frac{\Delta t (p_R - p_L)}{(\rho \Delta n)_L + (\rho \Delta n)_R}$$

$$p^* = \frac{(\rho c)_L p_R + (\rho c)_R p_L}{(\rho c)_L + (\rho c)_R} + q$$

In this scheme, q is the artificial viscosity of von Neumann

$$q = \begin{cases} 0 & \text{if } u_R - u_L \geqslant 0 \\ \frac{1}{2} b^2 (\rho_R + \rho_L)(u_R - u_L)^2 & \text{else} \end{cases}$$

where Δn is the distance from the cell center to the corresponding cell edge, and b is the artificial viscosity constant.

The MFCAV scheme attempts a compromise by combining the merits of both the WWAM and artificial viscosity methods, and exhibits good performance for material interfaces.

3.1.3. Dukowicz's two-shock Riemann scheme (DKWZ) [3]. In 1985 Dukowicz presented an approximate Riemann solver based on the shock relation, and a rarefaction wave is replaced by a shock wave in his formula. The DKWZ scheme is based on the following approximation through the shock Hugoniot relation:

$$p^* - p_s = \rho_s [a_s + A_s |u^* - u_s|](u^* - u_s) \tag{7}$$

where the subscript s refers to the left or the right state, and a_s and A_s are two material-dependent parameters

$$a_s = \sqrt{\left(\frac{\partial p}{\partial \rho} + \frac{p}{\rho^2} \frac{\partial p}{\partial e} \right)_s}$$

is the local isentropic speed of sound, and

$$A_s = \lim_{\text{strong shock}} \left[\frac{\rho_2 / \rho_1}{\rho_2 / \rho_1 - 1} \right]_s$$

DOI: 10.1002/fld

is a strong shock parameter that is given in terms of the density ratio across a shock in the strong shock limit. Typically, this parameter does not depart greatly from unity, because for materials with $p=p(\rho)$ it can be shown that $A_s=1$, while for polytropic (ideal gas) equations of state $A_s=\frac{1}{2}(\gamma+1)$. With the left and right states, Equation (7) make up a set of quadratic equations, and the quadratic nonlinearity enables the DKWZ scheme to deal with a large range of conditions from weak sound waves to strong shocks. However, numerical oscillations may appear in the vicinity of material interfaces when using the DKWZ scheme.

3.2. New adaptive Riemann solvers for general equation of state

As for the above three Riemann solvers, the WWAM scheme is obtained from the sound wave approximation; hence, it is easy to see that the scheme has larger numerical dissipation but less computation expense. Owing to the artificial viscosity in the MFCAV scheme, it could be expected that the scheme will suffer from the same problem of excessive numerical dissipation as common artificial viscosity methods do for shock waves. In addition, we can expect that the DKWZ scheme performs well for shock waves due to its double-shock wave approximation. It is our aim to develop a Riemann solver that can share the merits of the three schemes. Let us first compare and analyze the numerical features of the above three schemes through a Sod shock tube problem with initial conditions:

$$\rho=1,\ \ u=0,\ \ p=1 \quad \text{if } x\leqslant 0.5, \quad \rho=0.125,\ \ u=0,\ \ p=0.1 \quad \text{if } x>0.5$$

which is a classical problem and often used to verify schemes. The computational domain is $[0, 1]$ with 200 mesh cells.

Computational results in Lagrangian formulation are shown in Figure 2. We observe that all the three schemes can capture shock, contact and rarefaction waves correctly, but subtle numerical features are observed, especially for the resolution of the shock wave and contact discontinuity. As shown in Figure 2, the WWAM scheme can get quite a smooth picture of flow structure, but the numerical dissipation is obviously too large. As for the MFCAV scheme, the contact discontinuity is sharply captured, but obvious numerical oscillation appears across the shock wave. If we take a larger artificial viscosity coefficient, the oscillation becomes slightly small but still exists. On the contrary, the DKWZ can capture shock well but exhibits quite a large jump near contact discontinuity.

Another test example is the Lax problem with initial conditions:

$$\rho=0.445,\ \ u=0.698,\ \ p=3.528 \quad \text{if } x\leqslant 0.5, \quad \rho=0.5,\ \ u=0,\ \ p=0.571 \quad \text{if } x>0.5$$

The computed density in Eulerian formulation is plotted in Figure 3 with the three schemes. Owing to large numerical dissipation in Eulerian formulation, the solutions of the three schemes are smoother than those in Lagrangian formulation. However, we can still observe the numerical oscillations in the vicinity of the shock wave for the MFCAV scheme and the jumps across the contact discontinuity for the DKWZ and WWAM schemes.

The above numerical tests and analysis show that each scheme has its advantages and disadvantages. It will be an illuminative way if we can integrate the merits of the three schemes in one Riemann solver. Thus, we construct two adaptive Riemann solvers for general equations of state based on the different combinations of the three schemes, WWAM, MFCAV and DKWZ. We will apply adaptive treatment in our new schemes, such that they exhibit the feature of the MFCAV

DOI: 10.1002/fld

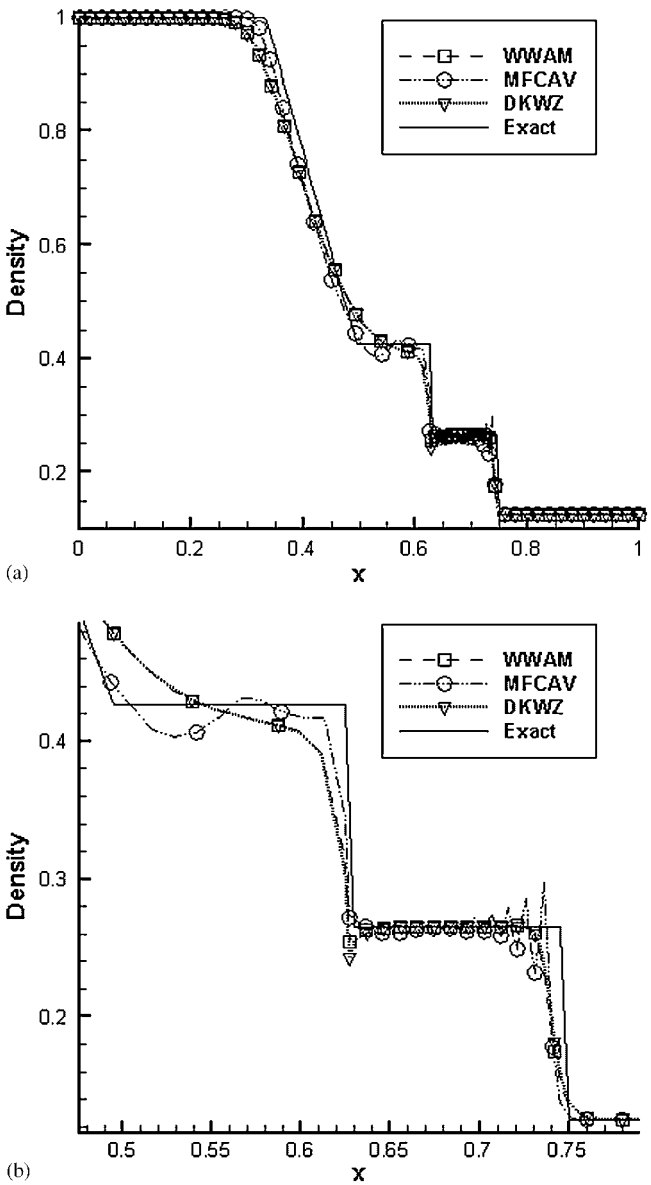

Figure 2. Comparison of Lagrangian computation results (MFCAV, DKWZ, WWAM and exact solution) at $t = 0.14$, Sod's problem, 200 cells: (a) density distribution and (b) density distribution (zoomed at contact and shock).

scheme at material interfaces, the feature of the DKWZ scheme at shock waves and the feature of the WWAM scheme in smooth flow regions.

According to different criteria of identifying elementary waves of the Euler equations, we present two adaptive Riemann solvers, i.e. the ARS1 and ARS2 schemes. Suppose that ρ_L, p_L, u_L

DOI: 10.1002/fld

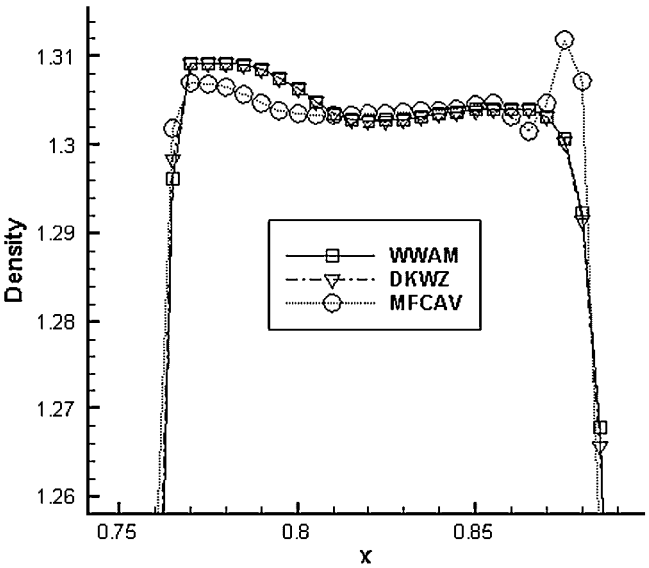

Figure 3. Lax's problem by the three schemes, at $t=0.16$, 200 cells. Left jump: contact discontinuity and right jump: shock wave (Lagrangian).

and ρ_R, p_R, u_R are the initial density, pressure and velocity of the Riemann problem on the left- and right-hand sides of a cell edge, respectively. Then, our Riemann solvers are illustrated as follows.

3.2.1. Adaptive Riemann solver 1 (ARS1) scheme

$$\text{ARS1}=\begin{cases}\text{WWAM} & \text{if } p^{**}\leqslant p_{\min}\\ \text{DKWZ} & \text{else if } u_R-u_L<\varepsilon\\ \text{MFCAV} & \text{else}\end{cases}$$

where $p_{\min}$ is the minimum of p_L, p_R, p^{**} is obtained by the WWAM scheme, and ε, instead of zero, is a small negative number, which is added due to the consideration of numerical stability, and often taken as $-1d-5$ if there is no special statement. The ARS1 scheme selects different Riemann solvers according to the variation of the pressure and velocity of flow field. Using the computed result p^{**} by WWAM as initial estimation, we can determine the structure of the Riemann problem. When $p^{**}\leqslant p_{\min}$, this means that both left and right waves are rarefaction waves; thus, the WWAM scheme is simply adopted. As is well known, across a shock wave the velocity decreases; we use the DKWZ scheme in this case. In the other situations, including the case of contact discontinuities, the MFCAV scheme is adopted.

3.2.2. Adaptive Riemann solver 2 (ARS2) scheme. In this scheme, we give another criterion to identify the contact, shock waves and smooth regions. This scheme is based on a suitable weight of the WWAW, DKWZ and MFCA schemes.

DOI: 10.1002/fld

Denote

$$\alpha=\left|\frac{p_{\mathrm{L}}-p_{\mathrm{R}}}{p_{\mathrm{L}}+p_{\mathrm{R}}}\right|,\quad \beta=\left|\frac{\rho_{\mathrm{L}}-\rho_{\mathrm{R}}}{\rho_{\mathrm{L}}+\rho_{\mathrm{R}}}\right|$$

Then, our weighted Riemann solver is expressed as

$$p^*=\frac{\alpha p^*_{\mathrm{DKWZ}}+\beta p^*_{\mathrm{MFCAV}}+\gamma p^*_{\mathrm{WWAM}}}{\alpha+\beta+\gamma},\quad u^*=\frac{\alpha u^*_{\mathrm{DKWZ}}+\beta u^*_{\mathrm{MFCAV}}+\gamma u^*_{\mathrm{WWAM}}}{\alpha+\beta+\gamma}$$

where the subscript denotes the results obtained by the relevant scheme, and γ is a small positive constant, usually equal to 0.1, and this choice is used for all the numerical examples of this paper.

In the ARS2 scheme, both the pressure ratio and the density ratio are considered to select schemes. When the pressure ratio is large, it is very possible that a shock wave exists. Hence, the DKWZ scheme plays a dominant role with a large weight α. In the vicinity of contact discontinuity, the density ratio is large; hence, the MFCAV scheme plays a dominant role with a large β. In the smooth regions, α and β are very small due to the small pressure and density ratios, and the WWAM scheme plays a dominant role.

To check the accuracy of the different approximate Riemann solvers, we compute a series of static Riemann problems with initial conditions

$$\rho_{\mathrm{L}}=1+k\Delta,\ p_{\mathrm{L}}=1+k\Delta,\ u_{\mathrm{L}}=k\Delta,\quad \rho_{\mathrm{R}}=1,\ p_{\mathrm{R}}=1,\ u_{\mathrm{R}}=0,\quad \Delta=0.2,\ k=-4\text{ to }66$$

where with different k, different Riemann problems are obtained. These Riemann problems are then solved using the above-mentioned three and our Riemann solvers. The computed results are given in Tables I and II, also in Figure 4. When $k\Delta$ is small, there is little difference among these solvers. With increase in $k\Delta$, the difference becomes large, and the MFCAV gives a higher pressure, whereas the WWAM gives a lower pressure. Overall, the ARS1 and ARS2 schemes take the advantages of the other three schemes and give in general more accurate numerical results in comparison with the exact solution.

Table I. Pressure by different Riemann solvers.

$K^*\Delta$	Exact	MFCAV	WWAM	DKWZ	ARS1	ARS2
−0.8	0.2616	0.3333	0.1756	0.2871	0.1756	0.2913
0.2	1.2310	1.1019	1.2200	1.2400	1.2400	1.2274
1.2	2.8569	1.9510	2.3512	3.1186	3.1186	3.0125
2.2	5.4912	4.0648	3.5071	6.3078	6.3078	6.1039
4.2	14.6623	15.3484	5.8454	17.2424	17.2424	17.0702
6.2	29.9309	41.1571	8.1974	34.8172	34.8172	35.3936
8.2	51.9279	87.5349	10.5551	59.4476	59.4476	62.0010
10.2	81.0347	160.4971	12.9156	91.4079	91.4079	97.6887
12.2	117.5106	266.0502	15.2778	130.8978	130.8978	143.1843
13.0	134.2084	318.7417	16.2230	148.8377	148.8377	164.2835

DOI: 10.1002/fld

Table II. Velocity by different Riemann solvers.

$K^*\Delta$	Exact	MFCAV	WWAM	DKWZ	ARS1	ARS2
−0.8	−1.0314	−0.6968	−0.6968	−1.0855	−0.6968	−1.0501
0.2	0.1784	0.1859	0.1859	0.1726	0.1726	0.1738
1.2	0.9748	1.1419	1.1419	0.9242	0.9242	0.9440
2.2	1.7236	2.1189	2.1189	1.6671	1.6671	1.7082
4.2	3.2388	4.0951	4.0951	3.2189	3.2189	3.2986
6.2	4.8140	6.0829	6.0829	4.8384	4.8384	4.9516
8.2	6.4412	8.0755	8.0755	6.5034	6.5034	6.6463
10.2	8.1079	10.0705	10.0705	8.2008	8.2008	8.3708
12.2	8.1079	10.0705	10.0705	8.2008	8.2008	8.3708
13.0	10.4902	12.8658	12.8658	10.6174	10.6174	10.8218

In the MFCAV scheme, the velocity is calculated in the same way as that for the WWAM scheme, since the mesh size and time step are not available for the MFCAV scheme in this static Riemann problem.

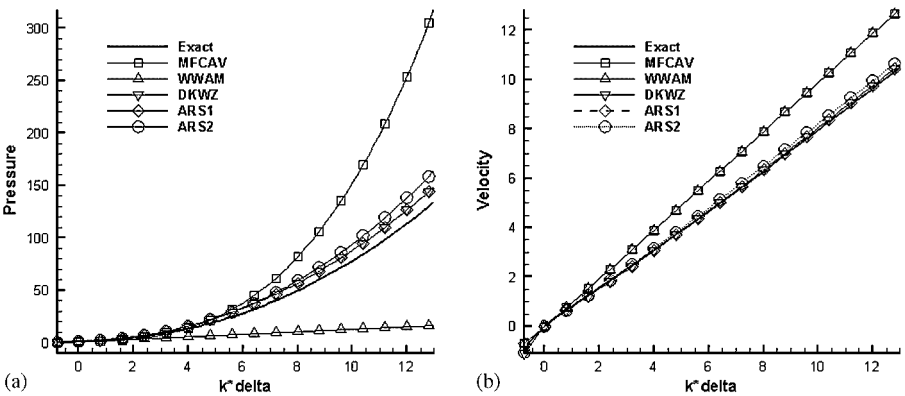

Figure 4. Static Riemann problem: (a) pressure and (b) velocity.

4. NUMERICAL EXAMPLES

In this section we present some numerical examples of multi-material flows, which have been tested in the literature by using different Riemann solvers, to validate our adaptive Riemann solvers for the numerical simulation of inviscid multi-material flows.

4.1. One-dimensional examples

4.1.1. Sod's shock problem. We consider Sod's shock tube problem in the unit interval with cell size $\Delta x = 0.005$. The Lagrangian numerical results are shown in Figure 5. It is obvious that both the ARS1 and ARS2 schemes give better numerical results than those obtained by the WWAM, MFCAV or DKWZ schemes shown in Figure 2. Moreover, the flow field obtained by the ARS2 scheme is slightly smoother than that obtained by the ARS1 scheme. This is mainly due to the fact that the ARS2 scheme is more diffusive than the ARS1 scheme.

DOI: 10.1002/fld

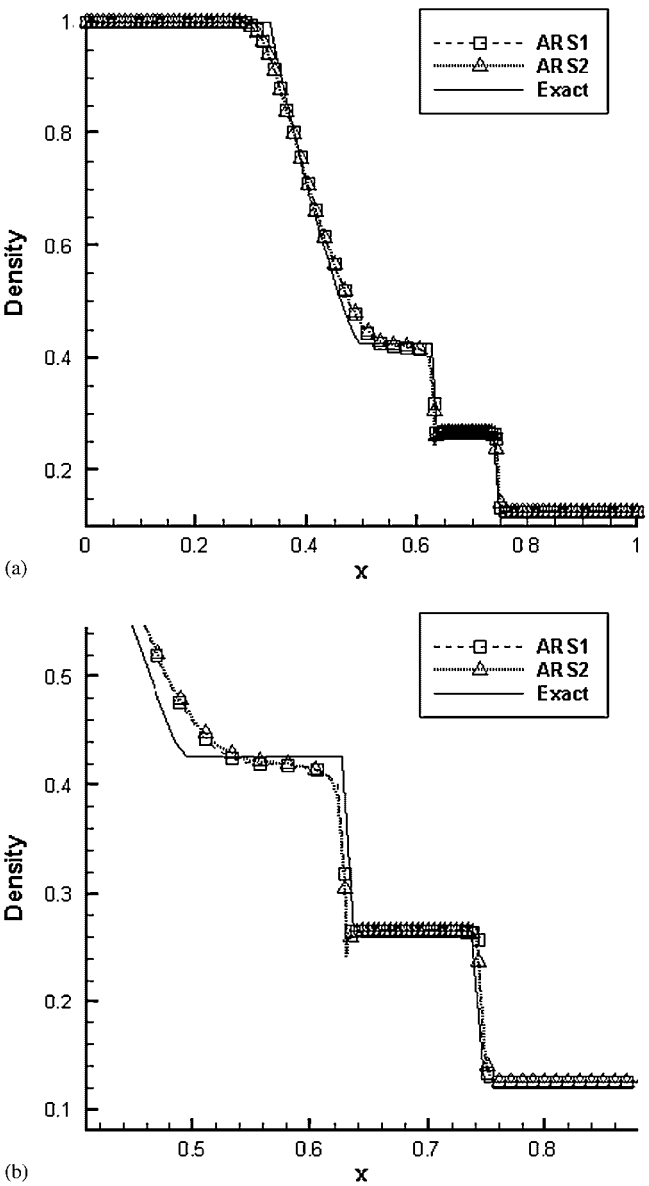

Figure 5. Sod's problem using the ARS1 and ARS2 scheme at $t=0.14$ Lagrangian, 200 cells: (a) density distribution and (b) density distribution (zoomed).

The L_1 and L_∞ errors of the ARS1 and ARS2 schemes are shown in Tables III and IV with different grids in Lagrangian formulation. A detailed error computation formula can be found in Reference [24]. From the tables we can see that both schemes have obtained a roughly first-order accuracy. In the finest mesh (800), the ARS1 scheme exhibits a slightly better accuracy than the ARS2 scheme through the comparison of L_∞ error.

DOI: 10.1002/fld

Table III. L_1 error and L_∞ error of ARS1 scheme for density.

Mesh cells	L_1 error	L_1 rate	L_∞ error	L_∞ rate
100	1.2697E−2	—	9.0541E−2	—
200	8.1903E−3	0.6325	8.2170E−2	0.1400
400	5.0550E−3	0.6962	7.4231E−2	0.1466
800	3.0534E−3	0.7273	4.9618E−2	0.5812

Table IV. L_1 error and L_∞ error of ARS2 scheme for density.

Mesh cells	L_1 error	L_1 rate	L_∞ error	L_∞ rate
100	1.3142E−2	—	8.9480E−2	—
200	8.0824E−3	0.7013	8.0906E−2	0.1453
400	4.9571E−3	0.7053	6.9724E−2	0.2146
800	2.9922E−3	0.7283	6.6797E−2	0.0619

4.1.2. Lax's problem. The computed results by the ARS1 and ARS2 schemes for Lax's problem are given in Figures 6(a)–(c) in Eulerian formulation with 400 mesh cells. Figure 6(c) shows the comparison for different schemes near the contact discontinuity. We see that both shock and contact waves are resolved well and are in good agreement with the exact solution. From Figure 3 we observe that the MFCAV and DKWZ schemes exhibit obvious spurious oscillations at shock wave and contact discontinuity, respectively, while our new schemes suppress these oscillations, combine the merits of these schemes and resolve both shock wave and contact discontinuity well. We point out here that in the first a few time steps of simulation, the shock, contact and rarefaction waves are not separated; hence, it is hard to select a suitable scheme. Here a special treatment is used for our adaptive schemes, namely, the MFCAV scheme is used for a few time steps at the beginning to produce the initial data for the ARS1 and ARS2 schemes.

4.1.3. Woodward–Colella interacting shock wave problem. The interacting shock wave problem was first featured as part of a test suite in [25]. It is a very challenging problem for numerical methods as the compressions are exceptionally high in very small volumes. It reflects some of the features of the 'peak' shock tube problems, and features strong nonlinear effects through the interaction of shocks, rarefaction waves and contact discontinuities.

The one-dimensional interacting shock wave problem consists of two separate shock tube problems featuring a region of low pressure in the middle, the fluid is a perfect gas with $\gamma=1.4$. At $t=0$, the density, velocity and pressure are taken to be

$$(\rho, u, p)=(1, 0, 1000) \quad \text{if } x\in[0, 0.1), \quad (\rho, u, p)=(1, 0, 0.01) \quad \text{if } x\in[0.1, 0.9)$$

$$(\rho, u, p)=(1, 0, 100) \quad \text{if } x\in[0.9, 1]$$

The boundary conditions at $x=0$ and 1 are set to be solid-wall conditions. For a more detailed description of this problem and its evolution, see [25]. The results at $t=0.038$ are given in Figure 7(a) with 800 grid points in Eulerian formulation. Figure 6(b) is Greenough and Rider's [26] results computed by the fifth-order WENO and second-order PLMDE methods, where the solid line is the result obtained using 1600 points and the other two are of using 800 points. We

DOI: 10.1002/fld

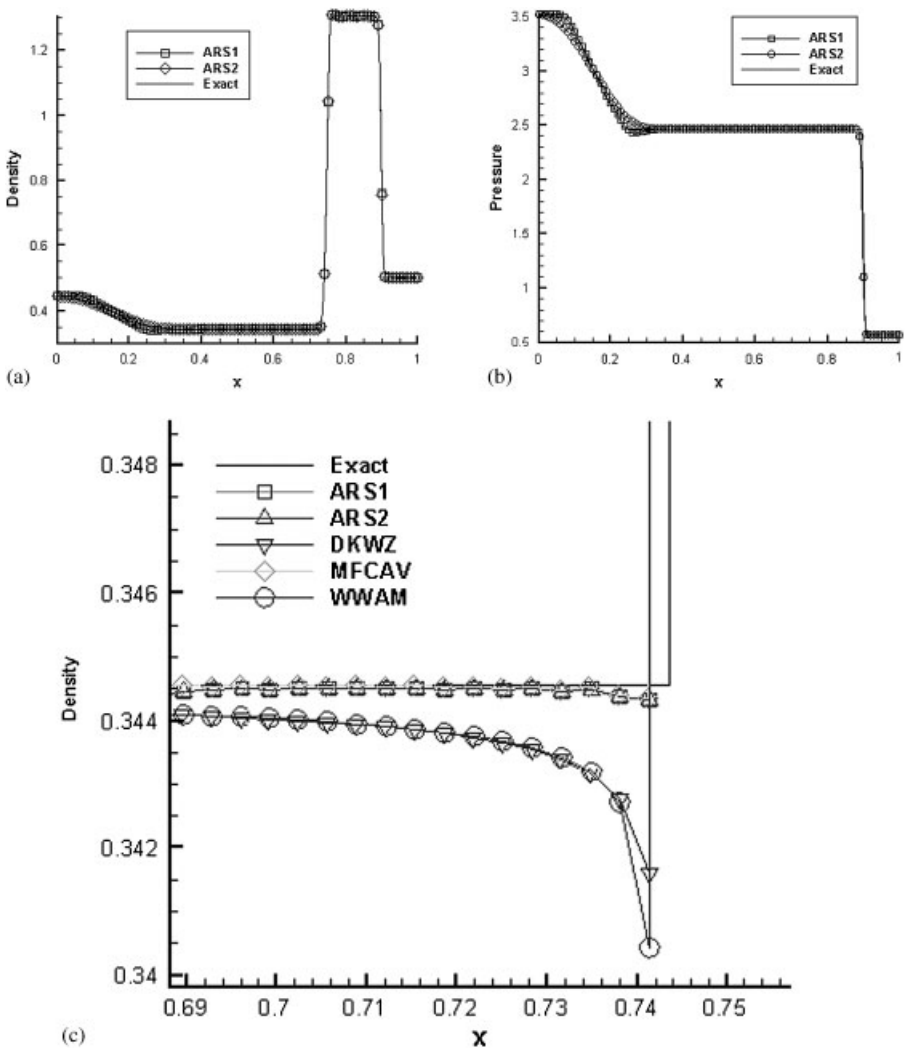

Figure 6. Lax's shock tube problem, 400 cells (Eulerian): (a) density, 400 cells; (b) pressure, 400 cells; and (c) resolution near contact discontinuity (left) and shock wave (right).

can see that the result obtained by the first-order scheme ARS1 is generally in good agreement in the large-scale structure with that in Reference [26] by the high-order schemes. This shows the capacity of our schemes for simulating strong shock, contact and rarefaction waves. Moreover, less CPU time is consumed by our method.

4.1.4. Double rarefaction wave problem. This example has the initial data:

$$\rho=1.0,\ \ u=-2,\ \ p=0.4 \quad \text{if } x\leqslant 0.5, \qquad \rho=1.0,\ \ u=2,\ \ p=0.4 \quad \text{if } x>0.5$$

DOI: 10.1002/fld

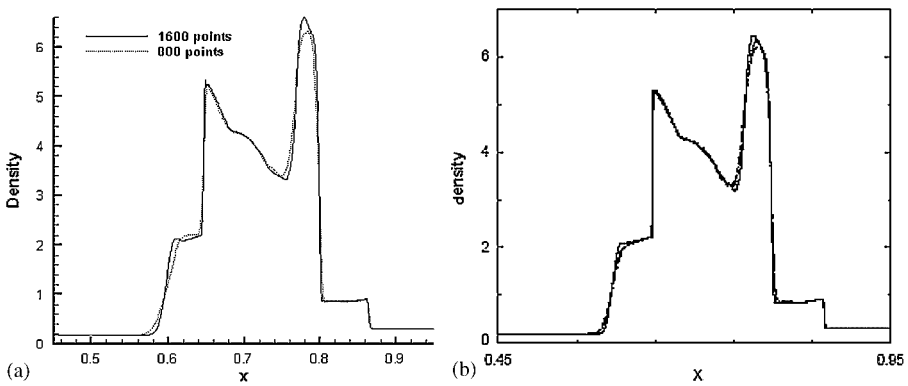

Figure 7. Woodward–Colella's interacting shock wave problem at $t = 0.038$, (Eulerian): (a) ARS1, 800 cells and (b) WENO5 and PLMDE method of Reference [26].

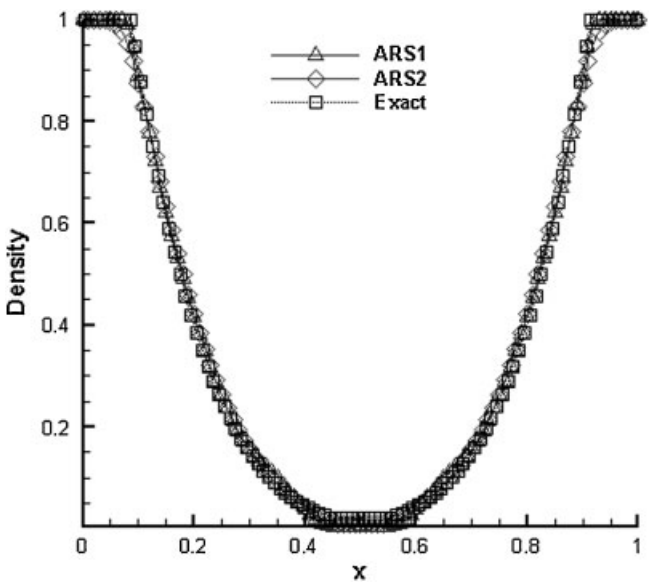

Figure 8. Double rarefaction problem $t = 0.15$, ARS1, ARS2, 400 cells, Eulerian.

This test, also called 123 problems, has solution consisting of two strong rarefactions and a trivial stationary contact discontinuity. The pressure is very small (close to vacuum), and a number of methods are known to have difficulties with this kind of symmetric Riemann problems [6]. Figure 8 shows results obtained with the ARS1 and ARS2 schemes (400 meshes used) in Eulerian formulation. It is easy to see that both rarefaction waves are resolved well, and the ARS2 scheme possesses slightly larger numerical dissipation.

DOI: 10.1002/fld

4.1.5. Double shock wave problem. The example has the initial data:

$$\rho=1.0,\ \ u=0,\ \ p=0.01 \quad \text{if } x\leqslant 0.5, \qquad \rho=1.0,\ \ u=0,\ \ p=100 \quad \text{if } x>0.5$$

This example with a very large pressure ratio is designed to test the robustness of numerical methods. The solution contains a left shock, a contact discontinuity, and a right shock, as shown in Figure 9 (400 meshes used) in Eulerian formulation. We see that the numerical results by the ARS1 and ARS2 schemes are generally in good agreement with the exact solution. This demonstrates the robustness of our schemes (Figure 9).

4.1.6. Gas–liquid shock tube problem. Now, we consider a gas–liquid shock tube test using the stiffened equation of state, taken from [27]. The initial conditions, corresponding to a water–air shock tube, are given by

$$(\rho, u, p, \gamma, p_\infty)_{\mathrm{L}}=(1000, 0, 10^9, 4.4, 6\times 10^8) \quad \text{if } x\leqslant 0.5$$

$$(\rho, u, p, \gamma, p_\infty)_{\mathrm{R}}=(50, 0, 10^5, 1.4, 0) \quad \text{if } x>0.5$$

This is a very difficult example with a large difference of material property. The left material is a liquid obeying the stiffened equation of state ($p+\gamma p_\infty=(\gamma-1)\rho e$), whereas the right material is an ideal gas. The numerical results by the ARS1 scheme in Lagrangian formulation are shown in Figure 10. Comparing with the exact solution obtained using a very fine mesh (3200 mesh cells), we see that the shock wave and material interface are resolved well though the pressure ratio is very large.

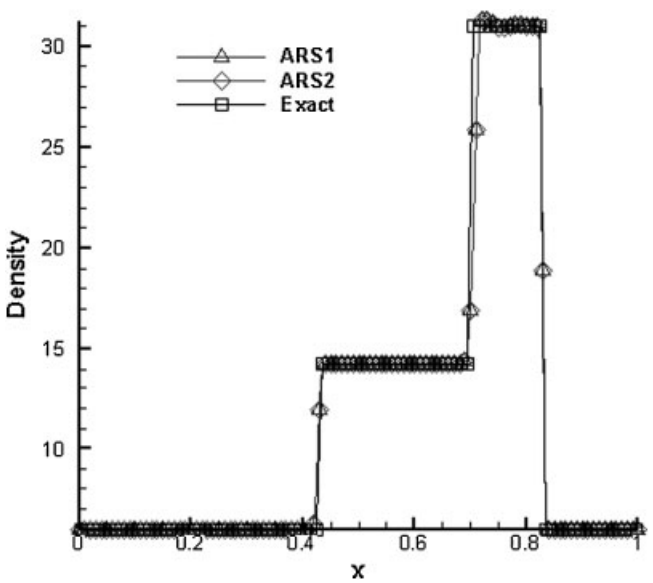

Figure 9. Double shock problem $t=0.035$, ARS1, ARS2, 400 cells, Eulerian.

DOI: 10.1002/fld

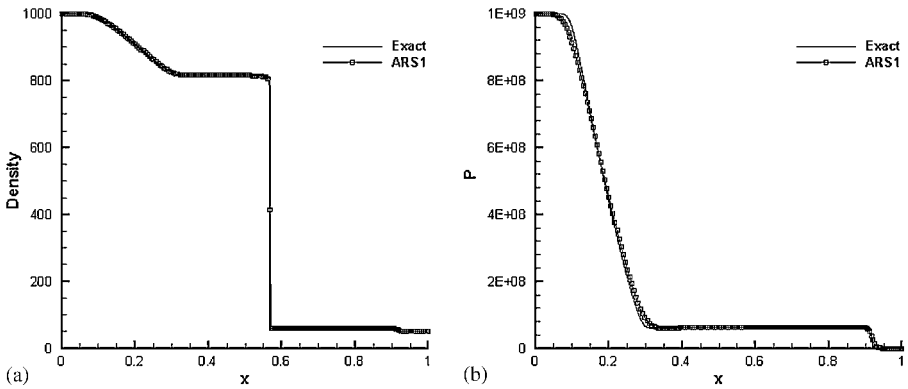

Figure 10. Gas–liquid shock tube problem, $t=0.00017$, ARS1, 800 cell points (Lagrangian): (a) density and (b) pressure.

4.2. Two-dimensional examples

4.2.1. Sedov's blast wave problem [*13*]. Consider a uniform medium in space with zero initial pressure. At time $t=0$, a fixed amount of energy is deposited at the origin, $r=0$. As time increases, a blast wave expands away from the origin. Because the initial pressure is zero, the shock associated with the blast wave is infinite in strength, and a similarity solution for the post shock profile can be obtained. The solution was first found by Sedov in 1959 for a γ-law gas and is particularly useful for testing the accuracy of multidimensional numerical schemes [13]. Here, we run a two-dimensional calculation and compare the numerical results obtained using the Riemann solvers discussed above.

An illustrative choice for a computational mesh is the one in which the plane coordinates are $\Delta x=\Delta y=1.1/N$ with N equal to 44 in a quadrant. A single unit of energy is deposited in the central cell of the mesh. According to the analytic theory, the blast shock wave should expand with radius equal to 1 at time $t=1$. The calculation is run in Lagrangian formulation with different Riemann solvers, and the corresponding density distributions are shown in Figure 11. The blast wave should be spherical at all times. We see that all the schemes can correctly reproduce the shape and position of the shock wave. The results computed by the DKWZ and WWAM schemes show slight asymmetry near the boundary. Owing to large numerical dissipation, the shock obtained by using the WWAM scheme is slightly smeared. The MFCAV scheme performs better than the other schemes in keeping the spherical symmetry, but the meshes are distorted due to numerical oscillations. The ARS2 scheme resolves better and preserves the spherical symmetry better than the DKWZ and WWAM schemes. From the numerical example we can see that the ARS2 scheme inherits the merits of the other three schemes.

The numerical results for the density using 44×44 cells in Lagrangian, ALE and Eulerian formulations are shown in Figure 12, where at $|x|=1$ the value of the analytic solution for the density is 6. We see that the Lagrangian result has the highest peak density due to its smallest numerical dissipation given by mesh movement with the fluid, whereas the Eulerian result has the lowest peak density due to its largest dissipation with fixed meshes among the three results. The ALE result lies between the Lagrangian and Eulerian results due to its suitable mesh movement. This implies that the ALE method makes a compromise by combining the merits of both Lagrangian and Eulerian methods, namely, more accurate than Eulerian methods in calculating discontinuities and more robust than Lagrangian methods in dealing with large deformation.

DOI: 10.1002/fld

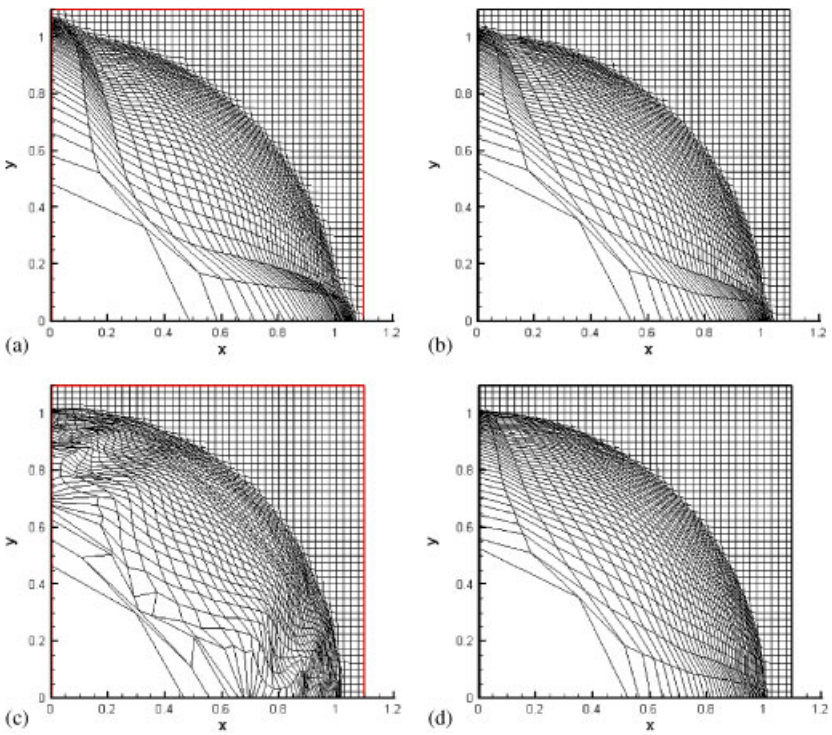

Figure 11. Sedov's blast wave problem at $t=1.0$, 44×44 cells (Lagrangian): (a) DKWZ; (b) WWAM; (c) MFCAV; and (d) ARS2.

4.2.2. Shock refraction problem. It is well known that a vortex sheet is generated by the interaction of a shock wave with an inclined interface that possesses a density discontinuity [20]. Because such interactions may be very complex, it is convenient to work with the so-called 'regular' refraction in which all waves are shock waves. For computational convenience we have chosen an interface between two ideal gases, both with $\gamma=1.4$. The nominal conditions specifying our test problem as shown in Figure 13(a) are incident shock Mach number (laboratory frame) $Ma=2$, interface density ratio $\rho_1/\rho_2=1.5$, and shock-interface angle of incidence equal to 60°.

The initial mesh is composed of two adjacent regions, each initially containing gases of different densities but equal pressures. Region 1 is a 36×30 mesh, with the left boundary vertical and the right boundary slanted at 60° to represent the interface. Region 2 is a 40×30 mesh uniformly slanted at 60°. The upper and lower boundaries are reflective, and the left boundary is a piston, which moves to the right with a velocity of 1.48 units, driving a Mach 2 shock into region 1.

The shock is allowed to propagate for a time $t=1.3$, and the results showing the density contours are given in Figure 13 for the WWAM, DKWZ and ARS2 schemes in Lagrangian formulation. As for the MFCAV scheme, the computation breaks down at about $t=0.75$ due to severe mesh distortion. It is observed that the WWAM scheme results in excessive numerical dissipation but almost without spurious oscillations. On the other hand, the DKWZ scheme leads to spurious oscillations near the lower part of the computation domain. Overall, the APRS scheme gives the clearest structure among these schemes.

DOI: 10.1002/fld

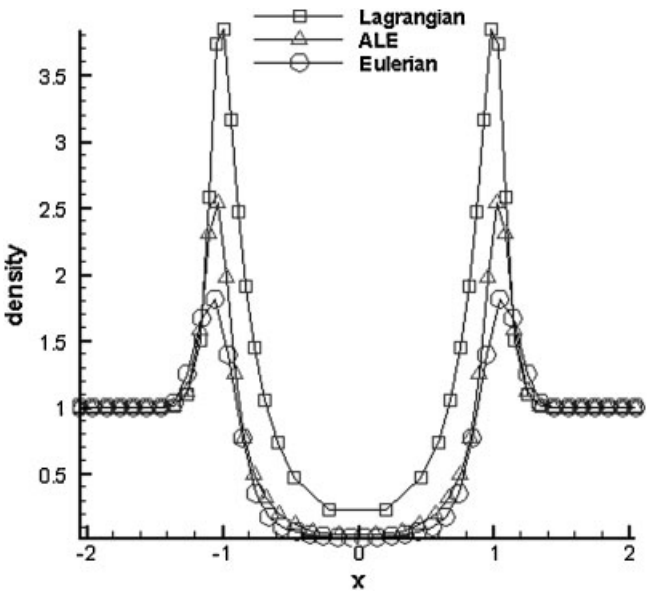

Figure 12. Sedov's blast wave problem in Lagrangian, ALE and Eulerian formulations.

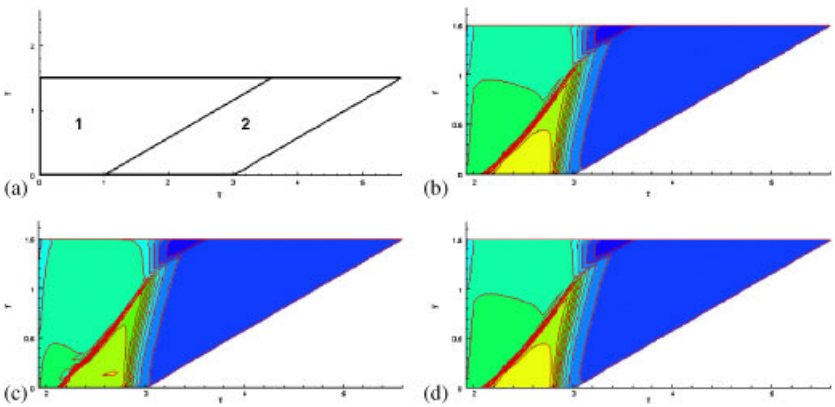

Figure 13. Shock interface interaction problem at $t=1.3$ (Lagrangian): (a) initial value; (b) WWAM; (c) DKWZ; and (d) ARS2.

4.2.3. Two-dimensional Riemann problem. This example is a two-dimensional Riemann problem with the initial data consisting of two shocks and two slip lines:

$$\begin{aligned}
&\rho=0.5313, \quad p=0.4, \quad u=0, \quad v=0 \quad \text{if } x>0, \quad y>0\\
&\rho=1.0, \quad p=1.0, \quad u=0, \quad v=0.7226 \quad \text{if } x>0, \quad y<0\\
&\rho=1.0, \quad p=1.0, \quad u=0.7226, \quad v=0 \quad \text{if } x<0, \quad y>0\\
&\rho=0.8, \quad p=1.0, \quad u=0, \quad v=0 \quad \text{if } x<0, \quad y>0
\end{aligned}$$

DOI: 10.1002/fld

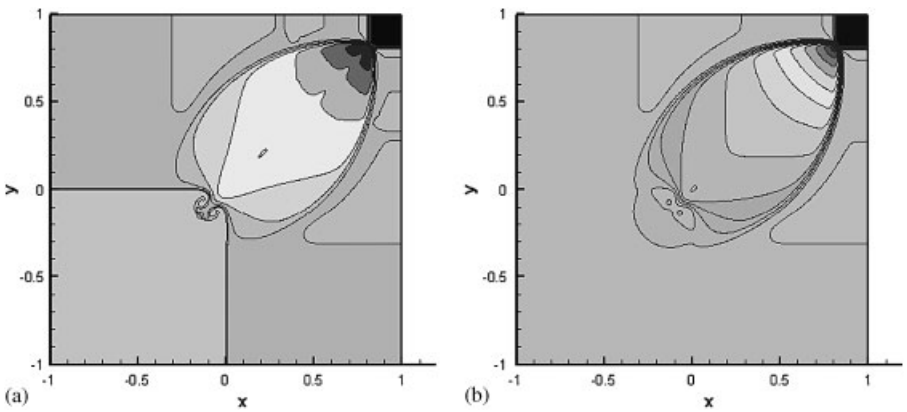

Figure 14. Two-dimensional Riemann problem, $t=0.52$, ARS1, 400×400 cells (Eulerian): (a) density and (b) pressure.

The computation is performed on a 400×400 grid using the ARS1 scheme in Eulerian formulation. The numerical contains a Mach reflection shown in Figure 14. This case was analyzed in [28], where it was demonstrated that the van Leer flux vector splitting scheme might produce a curved shock connected with two other shocks, resembling regular shock reflection, whereas our Riemann solver is able to resolve the solution as a Mach reflection. Moreover, our ARS1 solver gives more resolved spike structure than that in [28] by the two-dimensional wave solvers and demonstrates its capacity for computing shocks and contact discontinuities.

4.2.4. Double Mach reflection problem. For this problem the initial data are given by [28]

$$\begin{aligned}
&\rho=1.5,\quad p=1.5,\quad u=0,\quad v=0 && \text{if } x>0,\ y>0\\
&\rho=0.5323,\quad p=0.3,\quad u=0.0,\quad v=1.206 && \text{if } x>0,\ y<0\\
&\rho=0.5323,\quad p=0.3,\quad u=1.206,\quad v=0 && \text{if } x<0,\ y>0\\
&\rho=0.1379,\quad p=0.029,\quad u=1.206,\quad v=1.206 && \text{if } x<0,\ y<0
\end{aligned}$$

The common boundaries of the four quadrants are all shock waves. Thus, double Mach reflection phenomenon appears due to the interaction of shock waves with the initial data. Solutions are computed on a 400×400 grid to time $t=0.6$ by the ARS1 scheme in Eulerian formulation. Figure 15 shows the flow structure of the problem. We see that a mushroom cap structure is formed due to the interaction of the dense stream and postshock flow behind the oblique shock and that the simulated results here reproduce the large-scale structure of the corresponding numerical results in [28].

4.2.5. Stratified Richtmyer–Meshkov (RM) instability problem. RM instability arises when a material interface between two fluids with different densities is accelerated impulsively by an incident shock wave and plays an important role in many applications, such as inertial confinement fusion, supernova and so on [29]. Here, we present a numerical simulation of a stratified RM instability with two different equations of state.

DOI: 10.1002/fld

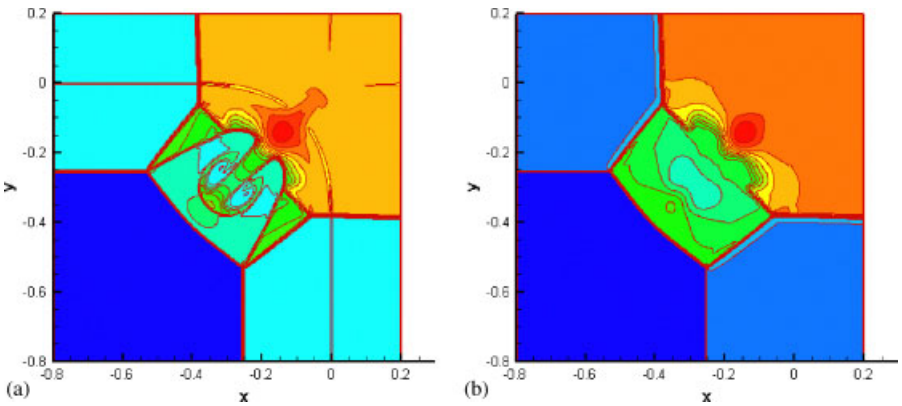

Figure 15. Double Mach reflection problem (ARS1) at $t = 0.6$, 400×400 cells (Eulerian): (a) density and (b) pressure.

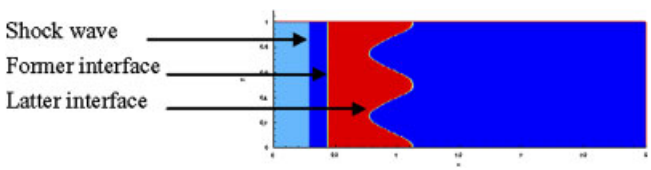

Figure 16. Initial configuration of stratified RM instability.

To set up the test, we consider a shock tube with length 3 and height 1. The initial condition in the tube is composed of a heavy fluid (the red one) sandwiched in light fluids as shown in Figure 16, and a shock wave with Mach number 2.02 approaches the interface from the left light fluid to the middle heavy fluid. The sandwiched heavy fluid has the ratio of specific heats 1.67 and the light fluid 1.4. It is known that the interface becomes unstable (i.e. the amplitude of the initial perturbation to the interface grows with time) after the passage of the shock wave. Simulation results are shown in Figure 17 by the ARS1 scheme in ALE formulation. It should be mentioned that a γ-model in [29] was used to treat the mixed cells of two gases in this example. We can see that the typical spike structure is formed due to the heavy fluid penetrating into the light fluid. Influenced by instability of the latter interface, the former interface is also distorted though it has no initial perturbation.

5. CONCLUSIONS

Approximate or exact Riemann solvers play a key role in Godunov-type methods. In this paper, we first analyze and compare the numerical features, such as the resolution for shock and contact waves, of three approximate Riemann solvers, MFCAV, DKWZ and WWAM, by numerical experiments. Then, on the basis of the analysis and comparison, we propose two new adaptive Riemann solvers for general equations of state by combining the merits of the aforementioned three Riemann

DOI: 10.1002/fld

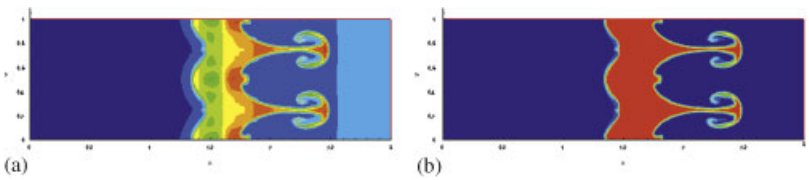

Figure 17. Results for the simulation of stratified RM instability, 400×120 cells (ALE): (a) density at $t = 2.0$ and (b) ratio of specific heats at $t = 2.0$.

solvers. Finally, based on the adaptive Riemann solvers, a Godunov-type ALE method is formulated to simulate compressible multi-material flows under large deformation. A number of numerical experiments confirm that the adaptive schemes well resolve both shock and contact waves, and are robust, accurate and very effective for general equations of state.

ACKNOWLEDGEMENTS

The authors are indebted to the referees for their useful suggestions that improved the presentation of this paper. This study was supported by the National Basic Research Program (Grant No. 2005CB321700), the NSFC (Grant No. 10225105), the Science Foundation of CAEP (Grant No. 20060648) and the Key Lab Foundation (9140C690101070C69).

REFERENCES

1. von Neumann, Richtmyer RD. A method for the numerical calculations of hydrodynamics shocks. *Journal of Applied Physics* 1950; **21**:232.
2. Godunov SK, Zabrodin AV, Prokopov GP. A difference scheme for numerical computation of discontinuous solution of hydrodynamic equations. *USSR Computational Mathematics and Mathematical Physics* 1961; **1**:1187 (English Translation).
3. Dukowicz JK. A general, non-iterative Riemann solver for Godunov's method. *Journal of Computational Physics* 1985; **61**:119.
4. Engquist B, Osher S. One side difference approximation for nonlinear conservation laws. *Mathematics of Computation* 1981; **16**(154):321–351.
5. Roe PL. Approximate Riemann solvers, parameters vectors, and difference schemes. *Journal of Computational Physics* 1981; **43**:357–372.
6. Toro EF. *Riemann Solvers and Numerical Methods for Fluid Dynamics*. Springer: Berlin, Heidelberg, 1999.
7. Li D, Xu G, Shui H, He G, Chen G, Yuan G. *Numerical Methods for Two-dimensional Unsteady Fluid Dynamics*. The Science Press: Beijing, 1987; 246.
8. Miller GH, Puckett EG. A high-order Godunov method for multiple condensed phases. *Journal of Computational Physics* 1996; **128**:134–164.
9. Rider WJ. An adaptive Riemann solver using a two-shock approximation. *Computers and Fluids* 1999; **28**: 741–778.
10. van Leer B. Towards the ultimate conservative difference scheme, V. A second order sequel to Godunov's method. *Journal of Computational Physics* 1979; **32**:101–136.
11. Colella P, Woodward PR. The piecewise parabolic method (PPM) in gas dynamical simulation. *Journal of Computational Physics* 1984; **54**:174–201.
12. Hirt CW, Amsden AA, Cook JL. An arbitrary Lagrangian–Eulerian computing method for all flow speeds. *Journal of Computational Physics* 1974; **14**:227.
13. Addessio FL, Baumgardner R, Dukowicz JK, Johnson NL, Kashiwa BA, Rauenzahn RM, Zemach C. CAVEAT: a computer code for fluid dynamics problems with large distortion and internal slip. *Los Alamos Report LA-10613-MS*, 1992.

DOI: 10.1002/fld

14. Darlington RM, McAbee TL, Rodrigue G. A study of ALE simulations of Rayleigh–Taylor instability. *Computer Physics Communications* 2001; **135**:58.
15. Shashkov M, Wendro B. The repair paradigm and application to conservation laws. *Journal of Computational Physics* 2004; **198**:265–277.
16. Benson DJ. Computational methods in Lagrangian and Eulerian hydrocodes. *Computer Methods in Applied Mechanics and Engineering* 1992; **99**:235.
17. Johnson L. The legacy and future of CFD. *Los Alamos 96-1426-LA-URN*.
18. Amsden AA, Ruppel HM, Hirt CW. SALE: a simplified ALE computer program for fluid flow at all speeds. *LA-8095UC-32*, Issued: June 1980.
19. Luo H, Baum JD, Löhner R. On the computation of multi-material flows using ALE formulation. *Journal of Computational Physics* 2004; **194**:304–328.
20. Dukowicz JK, Meltz JA. Vorticity errors in multidimensional Lagrangian codes. *Journal of Computational Physics* 1992; **99**:115–134.
21. Caramana EJ, Shashkov MJ. Elimination of artificial grid distortion and hourglass-type motions by means of Lagrangian subzonal masses and pressures. *Journal of Computational Physics* 1998; **142**:521–561.
22. Winslow AM. Adaptive mesh zoning by the equipotential method. *UCID-9062*, Lawrence Livermore National Laboratory, 1981.
23. Benson DJ. Momentum advection on a staggered mesh. *Journal of Computational Physics* 1992; **100**:143–162.
24. Greenough JA, Rider WJ. A quantitative comparison of numerical methods for the compressible Euler equations: fifth-order WENO and piecewise-linear Godunov. *Journal of Computational Physics* 2004; **196**:259–281.
25. Woodward P, Colella P. The numerical simulation of two-dimensional fluid with strong shocks. *Journal of Computational Physics* 1984; **54**:115–173.
26. Greenough JA, Rider WJ. A quantitative comparison of numerical methods for the compressible Euler equations: fifth-order WENO and piecewise-linear Godunov. *Journal of Computational Physics* 2004; **196**:259–281.
27. Abgrall R, Karni S. Computations of compressible multifluids. *Journal of Computational Physics* 2001; **169**: 594–623.
28. Brio M, Zakharian AR, Webb GM. Two-dimensional Riemann solver for Euler equations of gas dynamics. *Journal of Computational Physics* 2001; **167**:177–195.
29. Shuye KM. An efficient shock-capturing algorithm for compressible multicomponent problems. *Journal of Computational Physics* 1999; **142**:208–242.

DOI: 10.1002/fld